Polyhedron 200 (2021) 115119

Contents lists available at ScienceDirect

Polyhedron

journal homepage: www.elsevier.com/locate/poly

A redox cascade of NO_x^- complexes: Structures and nitrogen deoxygenation thermodynamics

Alyssa C. Cabelof [1], Alec M. Erny [1], Daniel M. Beagan, Kenneth G. Caulton *

Department of Chemistry, Indiana University, Bloomington, IN 47405, USA

ARTICLE INFO

Article history:
Received 9 December 2020
Accepted 19 February 2021
Available online 26 February 2021

Keywords:
DFT
Pincer
Nitrate
Deoxygenation

ABSTRACT

The pincer ligand PNNH contains pyridine with its ortho carbons bearing one tBu_2PCH_2 donor and one pyrazole donor. A DFT study of the energies and structures of $(PNNH)Mn(CO)_n(NO_x)$ (n = 0–2, x = 0–3) reveals thermodynamic preferences over the suite of compounds. In every NO_x case, the cis positioning of two carbonyls gives a more stable isomer than does the trans, which is understood as avoiding the trans conflict of two strong π acid ligands. The calculations also reveal a preference for nitrito (—ONO) linkage isomers over the nitro ($—NO_2$) alternative. Additionally, the calculations predict loss of one CO when the nitrosyl oxidation level is reached, forming the five-coordinate $(PNNH)Mn(CO)(NO)$. Nitrosyl ligand bending is evaluated with changing manganese coordination number, and diagnostic infrared frequencies are also discussed. We also investigate the thermodynamics of deoxygenation of the original coordinated nitrate. It is shown that reductive deoxygenations among these species are thermodynamically favored using a bis silyl dihydropyridazine reagent (oxygen removed as $O(SiMe_3)_2$).

1. Introduction

Highly oxidized elements, regardless of whether they are gases or highly water soluble, represent important anthropogenic pollutants [1–4]. One remedial strategy for carbon dioxide is deoxygenation and C—C bond formation to produce multi-carbon products. The highest oxidation state of nitrogen is found in nitrate, which is a metabolite from agricultural ammonia fertilizer and whose water solubility leads to accumulation of this nutrient in poorly drained bodies of water [5–8]. This triggers excessive algal growth, then oxygen depletion which results in aquatic "dead zones" [9]. Deoxygenation of nitrate is currently not as advanced as is deoxygenation of carbon dioxide [10–15], although some successes have been discovered in the last decade [16–23]. We address here the process of deoxygenation of nitrate into various reduced nitrogen oxidation states, ultimately to the terminal nitride stage. This total deoxygenation, followed by protonation, accomplishes the return of N resource to a value-added product, NH_3. We envision the fate of the oxygen to be abstracted by oxophilic silicon, which is delivered by an antiaromatic silyl amine reagent (Scheme 1a) proven to have this capability, 1,4-bis (trimethylsilyl)-1,4-diaza-2,5-cyclohexadiene (TMS_2Pz) [24–29]. This reagent formally delivers two uncharged $SiMe_3$ equivalents based on the pyrazine aromaticity regained following silyl transfer. Relevant goals considered here include the choice of a transition metal as an electrophilic activator and a carrier of an ancillary ligand which can additionally promote activation of nitrate. While electrophilic activation dictates high metal oxidation state, we probe here whether a low metal oxidation state can also contribute. This study focuses on design of complexes for systematic study of nitrate deoxygenations, incorporating several specific design characteristics illustrated in Scheme 1b.

With the choice of manganese, there is the benefit of earth abundant character of a generally underutilized transition metal. We chose a tridentate pincer ligand (Scheme 1b, PNNH), which must be robust against degradation by the deoxygenating agent. It has three distinctly different donors: a phosphorus carrying sterically bulky substituents to avoid potentially destructive aggregation to multi metal species, a pyridine, known to be redox active [30–32], and a pyrazole, chosen in part to position a reactive NH hydrogen nearby the coordinated substrate. By choice of Mn(+1), we are in a region of coordination chemistry where the 18 valence electron rule can be a useful predictive guide, and we use here Density Functional Theory (DFT) calculations to test how useful that predictive principle is. The remaining ligand incorporated at our reactive metal center is carbon monoxide, whose spectroscopic properties could be useful in experimental tests of these calculations. Additionally, CO is diagnostic of relatively electron rich or electron poor character of the metal to which they are attached: high ν_{CO} indicates the metal donates less well to the π* orbitals

* Corresponding author.
E-mail address: caulton@indiana.edu (K.G. Caulton).
[1] These authors contributed equally.

https://doi.org/10.1016/j.poly.2021.115119
0277-5387/

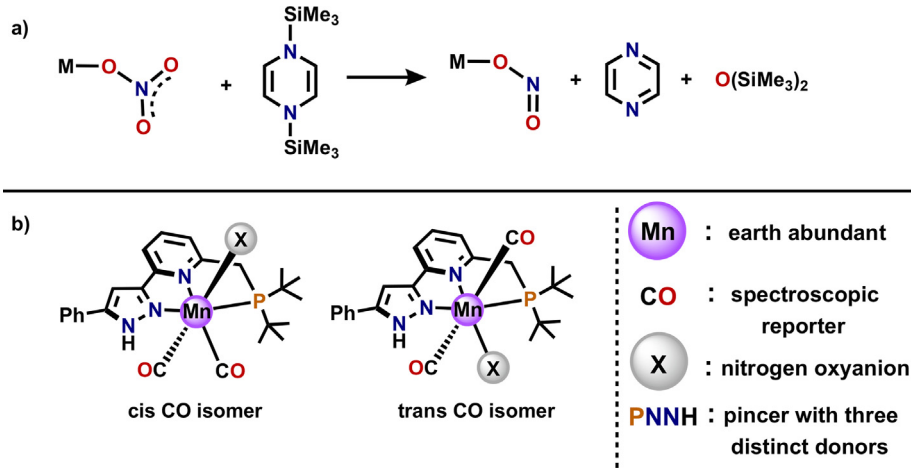

Scheme 1. a) Deoxygenation with TMS_2Pz b) complexes studied in this report with highlighted key features.

of CO vs. the low ν_{CO} values expected when the metal is electron rich. Part of this study seeks to track the changing electron donor or withdrawing character of nitrogen oxyanions as they are reduced. Ultimately, at the nitride stage, questions arise as to the accuracy of an M≡N triple bond representation and also whether higher spin states are relevant to these final deoxygenation products. In summary, the goals of this DFT study are to establish structure, bonding, and thermodynamics of isomeric products and deoxygenation steps, as well as to identify possible unanticipated degradative reactions, and unanticipated characteristics of the chosen pincer ligand. Given the limited access to nitride as a ligand (normally from high energy azide or from very refractory N_2), does the envisioned reductive silylation reagent TMS_2Pz have the thermodynamic capacity to produce nitride?

We analyze first the structures of the various nitrogen oxyanion complexes involved, followed by a general survey of the energetics of their interconversion by reductive silylation with TMS_2Pz.

2. Results

2.1. Structures of nitrogen oxyanion complexes

2.1.1. NO_3^- Complexes

We began our study with geometry optimization (B3LYP/6-311G(d) level of theory with implicit solvent corrections for THF solvent; see SI for more details) of $(PNNH)Mn(CO)_2(NO_3)$ for both the cis and trans isomer, based on the carbonyl positions. Calculations reveal that the cis isomer (Fig. 1a) is more stable than the trans isomer by 12.5 kcal/mol in spite of the fact that only the trans isomer shows an intramolecular hydrogen bond from NH to pendant κ^1-nitrate oxygen (Fig. 1b). The cis isomer is experimentally observed for manganese pincer complexes with a variety of X-type ligands [33–37].

Due to the cis being the more stable of the two isomers, discussion focuses on that isomer here, but more information on the trans isomer is available in the SI. DFT frequency calculations of the cis isomer reveal two strong CO stretches at 1871 cm^{-1} (*asym*) and 1940 cm^{-1} (*sym*). In addition to the CO as a spectroscopic reporter, nitrogen oxyanions are also excellent chromophores due to their distinct N—O stretches. These calculations predict that the N—O stretches for nitrate are at 1270 and 1448 cm^{-1}. These computed IR stretches are particularly useful to aid future synthetic efforts towards $(PNNH)Mn(CO)_2(NO_3)$ and for isomer identification vs. the experimental IR spectrum. It is noteworthy to mention that we envision the synthesis of this $(PNNH)Mn(CO)_2(NO_3)$ complex to be straightforward. Our group has installed PNNH onto multiple metals [24,38–40], and we therefore imagine that addition of PNNH to $Mn(CO)_5X$ will form $(PNNH)Mn(CO)_2X$ (X = Cl or Br) [36,37,41], which can subsequently undergo salt metathesis[37] with silver nitrate to form the desired $(PNNH)Mn(CO)_2(NO_3)$.

2.1.2. NO_2^- Complexes

In the case of nitrite, the first downstream product of nitrate deoxygenation, there are four possible isomers due to the ability of nitrite to be *N*-bound (nitro) or O-bound (nitrito), along with cis and trans $(CO)_2$ configuration. Geometry optimization of all four isomers was completed and shows that the cis CO with nitrito coordination is the most stable isomer. The relative energy of each isomer is shown in Fig. 2a, with the optimized structure of the most stable shown in Fig. 2b.

Similarly to the case of $(PNNH)Mn(CO)_2(NO_3)$, these calculations show that the cis isomer is more stable, despite a hydrogen

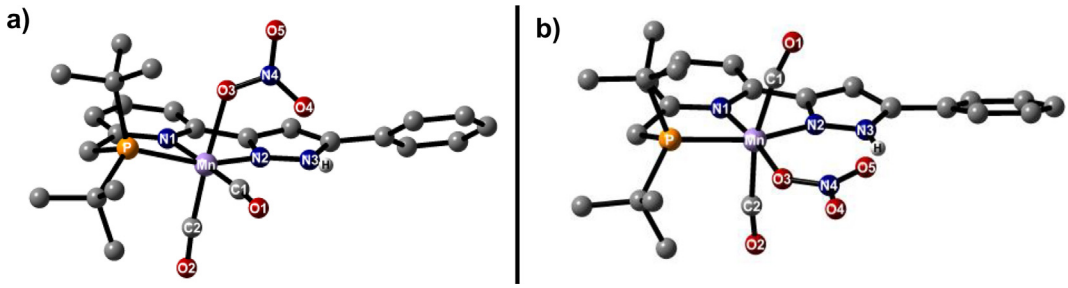

Fig. 1. Geometry optimized structures of $(PNNH)Mn(CO)_2(NO_3)$ as a) cis isomer b) trans isomer.

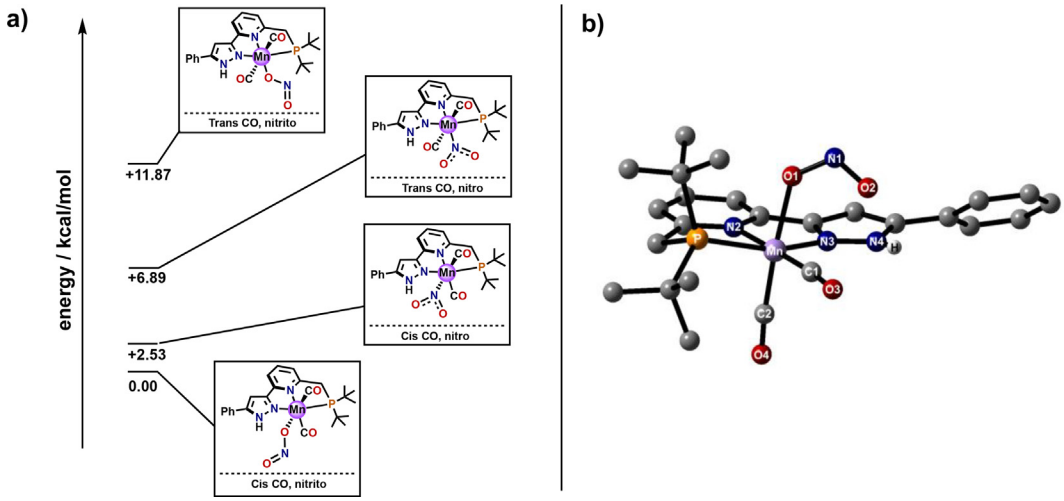

Fig. 2. a) Relative energies of all possible (PNNH)Mn(CO)$_2$(nitrite) isomers and b) Geometry optimized structure of cis-(PNNH)Mn(CO)$_2$(ONO).

bond between the nitrogen oxyanion and the pyrazole —NH proton only in the trans isomer. In all of these cases avoiding two mutually trans carbon monoxides dominates thermodynamic isomer preference in spite of hydrogen bonding opposing that preference. In general, hydrogen bonding only occurs when the nitrogen oxyanion is located in the plane of the pyrazole. For all isomers, the N—O stretches of nitrite are strongly mixed with pincer intraligand motions, and thus of limited diagnostic utility (see SI for more details). The carbonyl stretching modes on the other hand are the most intense in each spectrum and very useful; the symmetric stretch of the trans isomer is of low intensity, while the cis isomer has two of comparable intensity. These data are all included in the SI (Table S2).

2.1.3. Nitrosyl complexes

Upon reaching the nitrosyl state, we were interested in probing both (PNNH)Mn(CO)$_2$(NO) and (PNNH)Mn(CO)(NO), hypothesizing that upon formation the more strongly donating NO ligand, one CO might dissociate to give the five-coordinate alternative. We first focused on the dicarbonyl compounds, and then considered the thermodynamics for loss of carbonyl from the lowest energy dicarbonyl species. For the dicarbonyl species (PNNH)Mn(CO)$_2$(NO), we optimized both the cis and trans isomers and in line with the nitrate and nitrite results, the cis CO isomer is lower in energy, by 6.9 kcal/mol. For the cis isomer, the Mn—N—O angle is bent at 121.8°, consistent with sp^2 hybridization at N (Fig. 3a). Because we were interested in the monocarbonyl, we considered the thermodynamics to form (PNNH)Mn(CO)(NO) and free CO from cis-(PNNH)Mn(CO)$_2$(NO) and found that this process is favorable by 11.7 kcal/mol. The optimized structure of (PNNH)Mn(CO)(NO) is shown in Fig. 3b.

Due to the thermodynamics being downhill for formation of (PNNH)Mn(CO)(NO), unless there is an unanticipated barrier for this reaction, deoxygenation of (PNNH)Mn(CO)$_2$(NO$_2$) should spontaneously form the five-coordinate (PNNH)Mn(CO)(NO). The monocarbonyl has an essentially linear Mn—N—O angle of 168.2° and a square pyramidal geometry around five- coordinate manganese with an apical CO. The computed IR spectra of these two molecules suggests that differentiating these two species in a synthetic execution should be simple; if the dicarbonyl forms, the IR spectrum is dominated by the two CO stretches which are predicted to be much more intense than the nitrosyl. However, if CO loss occurs, DFT predicts that the nitrosyl stretch will be nearly as intense as the CO stretch (see SI for more details).

The linear (in (PNNH)Mn(CO)(NO)) vs. bent (119 – 122° in (PNNH)Mn(CO)$_2$(NO)) structural preferences (Fig. 3) are wholly consistent with the 18 electron rule and the demand for the metal here to remain saturated upon loss of one carbonyl ligand. The manganese nitrogen distance to bent nitrosyl is distinctly longer (by > 0.3 Å) than to linear nitrosyl. However, the bent nitrosyl exerts a trans lengthening on Mn-C(O) in the examples here. It is perhaps surprising that the five-coordinate species locates carbonyl, not nitrosyl, trans to the empty site in its square pyramidal structure. There are no known bent Mn—N—O complexes. There is one complex, cationic with a monoanionic pincer ligand L, with formula LMn(CO)$_2$(NO)$^+$; it has a linear MnNO unit [42].

2.1.4. Nitride complexes

We discuss first the five-coordinate (PNNH)Mn(CO)(N), predicting that this 18 electron species is preferred over the 20 valence electron dicarbonyl alternative. Additionally, our nitrosyl calculations suggest that CO loss from dicarbonyl will occur at that step.

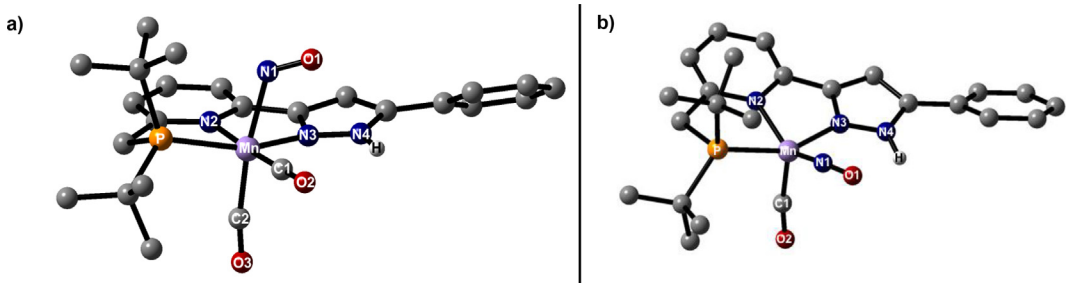

Fig. 3. a) Geometry optimized structure of cis-(PNNH)Mn(CO)$_2$(NO) b) geometry optimized structure of (PNNH)Mn(CO)(NO).

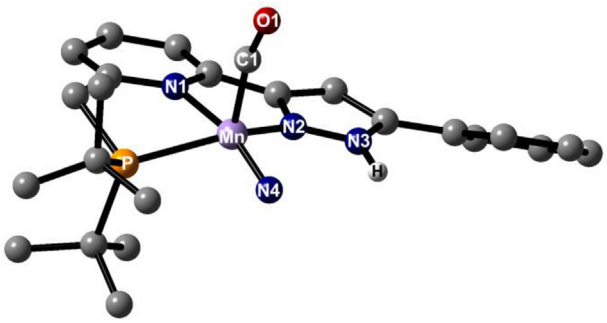

Fig. 4. Geometry optimized structure of (PNNH)Mn(CO)(N). ν_{CO} is 1843 cm^{-1}.

We considered all three possible spin states, and found the singlet to be lowest in energy by > 16 kcal/mol. The nitride is equatorial (Fig. 4) and shows a large trans influence, with Mn-N(pyridine) 2.208 Å, vs ~ 2.0 for the other NO_x species calculated here. The Mn—C(O) distance, 1.797 Å is short and the long CO distance, 1.158 Å, is consistent with back donation to CO, so this 18 valence electron S = 0 species has good bonding parameters. Consistent with that, the Mn—CO bond dissociation free energy (forming (PNNH)MnN) is >20 kcal/mol, considering all three spin states of (PNNH)MnN calculated here (see SI for more details).

There are numerous nitride complexes of Mn but all in oxidation state 5+, and commonly have the nitride ligand in the apical site [43–47]. There are also rhenium nitrides, including numerous with pincer ligands, but these also have primarily oxidation state 5 + [48–51]. There are no known M(N)(CO) complexes of manganese or rhenium.

2.2. Reductive silylation thermodynamics

We considered the reaction thermodynamics for stepwise and complete deoxygenation by TMS_2Pz, focusing on the lowest energy isomers determined above. The thermodynamics are summarized in Scheme 2 and reveal that deoxygenations are highly exergonic, even at the final deoxygenation step. These thermodynamic data support our initial hypothesis that the driving force for formation of free pyrazine and hexamethyldisiloxane help make these processes very favorable, and reveal the potency of TMS_2Pz as a deoxygenating agent. Here, we focus on nitrogen oxyanions, but we envision that these principles can be transferred to other oxyanions EO_n^{q-} (E = S, P, C, etc.).

2.3. Unanticipated reactions

2.3.1. From isonitrosyl

Because isomerization from nitrito to nitro is uphill thermodynamically (Scheme 2), we considered another route: deoxygenation of the nitrito species to form (PNNH)Mn$(CO)_2$(ON), which contains an isonitrosyl, and its subsequent isomerization to form (PNNH)Mn$(CO)_2$(NO). Attempted geometry optimization starting from (PNNH)Mn$(CO)_2$(ON) connectivity yielded an unexpected structure (Fig. 5), which reveals hydrogen transfer of pyrazole NH to the pendant isonitrosyl N. This gives the O-bound ligand HNO as a two electron donor, yielding a deprotonated and thus monoanionic pincer ligand of overall formula (PNN)Mn$(CO)_2$(ONH).

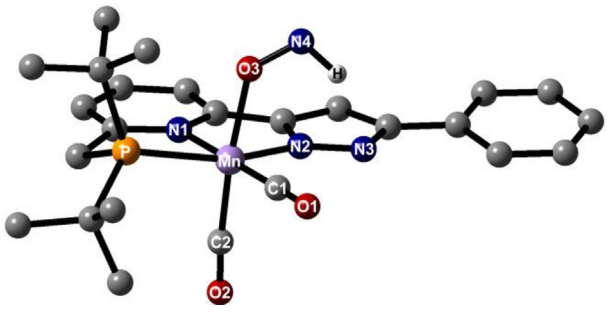

Fig. 5. Geometry optimized structure of (PNN)Mn$(CO)_2$(ONH).

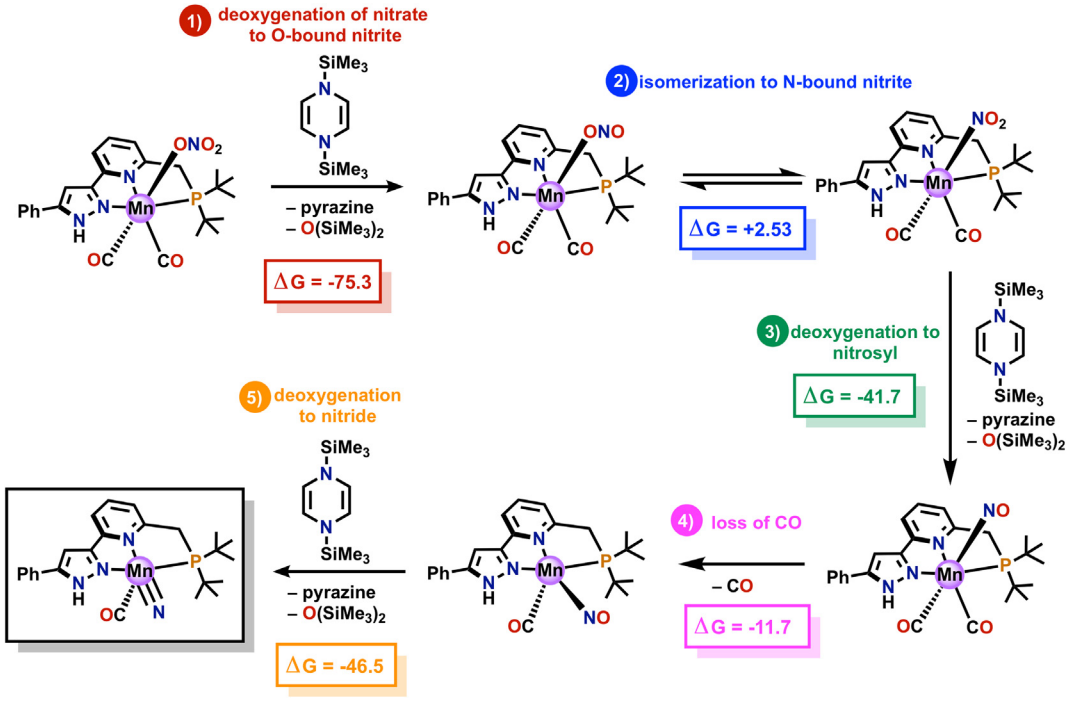

Scheme 2. Thermodynamics (energies in kcal/mol) of stepwise deoxygenations using TMS_2Pz.

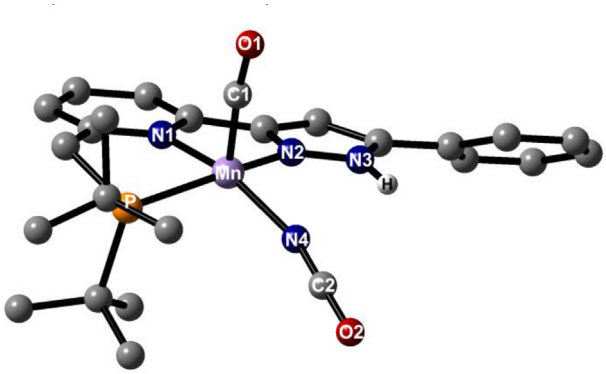

Fig. 6. Optimized structure of (PNNH)Mn(CO)(NCO). ν_{CO} is 1815 cm^{-1} ν_{NCO} is 2212 cm^{-1}.

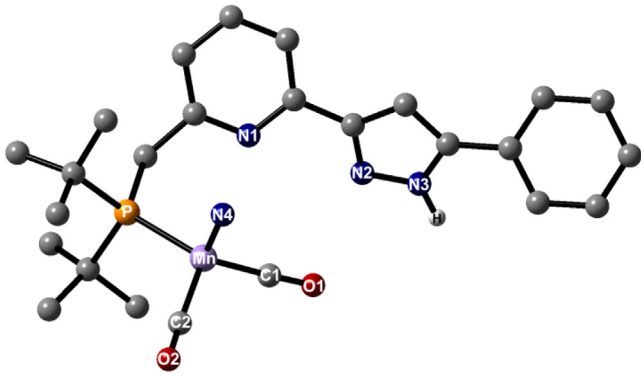

Fig. 7. Optimized structure of (κ^1-PNNH)MnN$(CO)_2$.

2.3.2. From dicarbonyl nitride

We were interested in attempted geometry optimization of these 20 valence electron species, (PNNH)Mn$(CO)_2$(N), both cis and trans, for comparison to the 18 valence electron (PNNH)Mn(CO)(N). The DFT geometry optimization revealed several unexpected products. Optimization starting from trans-(PNNH)Mn$(CO)_2$(N) led to coupling of one CO with the nitride ligand, forming five-coordinate (PNNH)Mn(CO)(NCO). (Fig. 6) Isocyanate formation from transition metal nitride reactivity with CO has been observed for several different metals [52–57]. This conversion to a 16 electron isomer shows that unsaturated is better than supersaturated, and also that the nitride is spontaneously *(i.e.* kinetically and thermodynamically) reactive towards functionalization (C/N bond formation) of nitrate-derived nitrogen. We find that (PNNH)Mn(CO)(NCO) is 51.3 kcal/mol more stable than (PNNH)Mn(CO)(N) + free CO, suggesting that this product is preferential to simple loss of CO.

Attempted optimization starting from cis-(PNNH)MnN$(CO)_2$ leads to dissociation of pincer arm(s). Specifically, manganese rejects donation from the pyridine and pyrazole donor arms, instead heading towards a four-coordinate structure of formula (κ^1-PNNH)MnN$(CO)_2$ with only the phosphine arm, both carbonyl and the nitride remaining in bonding distance of Mn (Fig. 7), and approximately tetrahedral structure around Mn. This molecule shows characteristic CO stretches at 1957 and 2016 cm^{-1} for the asymmetric and symmetric stretches respectively. The single precedent for a four-coordinate manganese nitride species is the tripodal (tris-NHC)MnN [58].

These optimizations both emphasize the predictive properties of the 18 valence electron rule; in both cases, significant geometry rearrangements occur to circumvent the high energy 20 valence electron species.

3. Conclusions

In every NO_x case, the cis positioning of two carbonyls gives a more stable isomer than does the trans, which is understood as avoiding the trans conflict of two strong π acid ligands. The nitrito isomer is more stable than the nitro isomer, which is surprising given that an O-bound ligand experiences filled/filled repulsions between d^6 manganese and the oxygen lone pairs. This suggests dominant influence of push/pull interaction, from O ligand lone pair into the π^* of CO which is absent in the nitro isomer. When the nitrosyl state is reached, satisfying its electronic demands dominate, and the increased valence electron count of linear nitrosyl vs. bent can be used to predict the favorable thermodynamics for loss of one carbonyl ligand: it is at the nitrosyl stage where coordination number five is first encountered. Similarly the nitride complex is favored to retain one carbonyl ligand, yielding an 18 valence electron species, (PNNH)Mn(CO)(N).

Knowing the energy landscape among isomers, as well as among redox partners, is essential to effective setting of goals in synthetic chemistry. Until the advent of DFT, thermodynamic data were only available following experimental evaluation of pure compounds which had already been synthesized, thus not useful in a predictive capacity. The energy landscape among NO_x ligands established here, together with nitrosyl and ultimately the difficultly accessible nitride ligand, is exceptionally challenging simply because of the many alternatives. DFT also delivers the experimentally useful vibrational frequencies of NO stretching, as well as those of the carbonyl ligands we intentionally include here as spectroscopic reporters; this is exceptionally useful in identifying compounds prior to single crystal diffraction structure determination. In addition, geometry search of the energy landscape is unbiased and thus can find unanticipated low barrier rearrangement products from a chosen starting geometry. Finally spin states present another parameter that can amplify the challenge of characterizing products in the NO_x deoxygenation landscape, yet are accessible by DFT. In conclusion, the study offered here can provide assistance to an experimental search for reducing the oxidation level of nitrogen oxyanions.

CRediT authorship contribution statement

Alyssa C. Cabelof: Conceptualization, Methodology, Investigation. **Alec M. Erny:** Conceptualization, Methodology, Investigation. **Daniel M. Beagan:** Investigation. **Kenneth G. Caulton:** Supervision, Funding acquisition.

Declaration of Competing Interest

The authors declare that they have no known competing financial interests or personal relationships that could have appeared to influence the work reported in this paper.

Acknowledgement

This work was supported by the Indiana University Office of Vice President for Research and the National Science Foundation by grant CHE-1362127. This research was supported in part by Lilly Endowment, Inc., through its support for the Indiana University Pervasive Technology Institute.

Appendix A. Supplementary data

Supplementary data to this article can be found online at https://doi.org/10.1016/j.poly.2021.115119.

References

[1] J.W.G. Cairney, A.A. Meharg, Environ. Pollut. 106 (1999) 169–182.
[2] E.M. Elliott, C. Kendall, S.D. Wankel, D.A. Burns, E.W. Boyer, K. Harlin, D.J. Bain, T.J. Butler, Environ. Sci. Technol. 41 (2007) 7661–7667.
[3] D.-P. Häder, A.T. Banaszak, V.E. Villafañe, M.A. Narvarte, R.A. González, E.W. Helbling, Sci. Total Environ. 713 (2020) 136586.
[4] R.J. Park, D.J. Jacob, B.D. Field, R.M. Yantosca, M. Chin, J. Geophys. Res. Atmos. 109 (2004).
[5] W.K. Dodds, W.W. Bouska, J.L. Eitzmann, T.J. Pilger, K.L. Pitts, A.J. Riley, J.T. Schloesser, D.J. Thornbrugh, Environ. Sci. Technol. 43 (2009) 12–19.
[6] M. Duca, M.T.M. Koper, Energy Environ. Sci. 5 (2012) 9726–9742.
[7] J.W. Erisman, M.A. Sutton, J. Galloway, Z. Klimont, W. Winiwarter, Nat. Geosci. 1 (2008) 636–639.
[8] J.N. Galloway, J.D. Aber, J.W. Erisman, S.P. Seitzinger, R.W. Howarth, E.B. Cowling, B.J. Cosby, BioScience 53 (2003) 341–356.
[9] R.J. Diaz, R. Rosenberg, Science 321 (2008) 926.
[10] Y.Y. Birdja, E. Pérez-Gallent, M.C. Figueiredo, A.J. Göttle, F. Calle-Vallejo, M.T.M. Koper, Nat. Energy 4 (2019) 732–745.
[11] C. Costentin, S. Drouet, M. Robert, J.-M. Savéant, Science 338 (2012) 90–94.
[12] R. Francke, B. Schille, M. Roemelt, Chem. Rev. 118 (2018) 4631–4701.
[13] A.J. Morris, G.J. Meyer, E. Fujita, Acc. Chem. Res. 42 (2009) 1983–1994.
[14] S. Nitopi, E. Bertheussen, S.B. Scott, X. Liu, A.K. Engstfeld, S. Horch, B. Seger, I.E. L. Stephens, K. Chan, C. Hahn, J.K. Nørskov, T.F. Jaramillo, I. Chorkendorff, Chem. Rev. 119 (2019) 7610–7672.
[15] J. Qiao, Y. Liu, F. Hong, J. Zhang, Chem. Soc. Rev. 43 (2014) 631–675.
[16] P.L. Damon, G. Wu, N. Kaltsoyannis, T.W. Hayton, J. Am. Chem. Soc. 138 (2016) 12743–12746.
[17] M. Delgado, J.D. Gilbertson, Chem. Commun. 53 (2017) 11249–11252.
[18] J.C. Fanning, Coord. Chem. Rev. 199 (2000) 159–179.
[19] C.L. Ford, Y.J. Park, E.M. Matson, Z. Gordon, A.R. Fout, Science 354 (2016) 741.
[20] J. Gwak, S. Ahn, M.-H. Baik, Y. Lee, Chem. Sci. 10 (2019) 4767–4774.
[21] J.-X. Liu, D. Richards, N. Singh, B.R. Goldsmith, ACS Catal. 9 (2019) 7052–7064.
[22] J. Shen, Y.Y. Birdja, M.T.M. Koper, Langmuir 31 (2015) 8495–8501.
[23] S. Xu, D.C. Ashley, H.-Y. Kwon, G.R. Ware, C.-H. Chen, Y. Losovyj, X. Gao, E. Jakubikova, J.M. Smith, Chem. Sci. 9 (2018) 4950–4958.
[24] A.C. Cabelof, V. Carta, C.-H. Chen, K.G. Caulton, Dalton Trans. 49 (2020) 7891–7896.
[25] J. Seo, A.C. Cabelof, C.-H. Chen, K.G. Caulton, Chem. Sci. 10 (2019) 475–479.
[26] D.M. Beagan, V. Carta, K.G. Caulton, Dalton Trans. 49 (2020) 1681–1687.
[27] T. Saito, H. Nishiyama, H. Tanahashi, K. Kawakita, H. Tsurugi, K. Mashima, J. Am. Chem. Soc. 136 (2014) 5161–5170.
[28] H. Tsurugi, K. Mashima, Acc. Chem. Res. 52 (2019) 769–779.
[29] H. Tsurugi, H. Tanahashi, H. Nishiyama, W. Fegler, T. Saito, A. Sauer, J. Okuda, K. Mashima, J. Am. Chem. Soc. 135 (2013) 5986–5989.
[30] T.R. Dugan, E. Bill, K.C. MacLeod, G.J. Christian, R.E. Cowley, W.W. Brennessel, S. Ye, F. Neese, P.L. Holland, J. Am. Chem. Soc. 134 (2012) 20352–20364.
[31] R.A. Lewis, K.C. MacLeod, B.Q. Mercado, P.L. Holland, Chem. Commun. 50 (2014) 11114–11117.
[32] C. Römelt, T. Weyhermüller, K. Wieghardt, Coord. Chem. Rev. 380 (2019) 287–317.
[33] N.H. Anderson, J.M. Boncella, A.M. Tondreau, Organometallics 37 (2018) 4675–4684.
[34] F. Bertini, M. Glatz, N. Gorgas, B. Stöger, M. Peruzzini, L.F. Veiros, K. Kirchner, L. Gonsalvi, Chem. Sci. 8 (2017) 5024–5029.
[35] S. Chakraborty, U. Gellrich, Y. Diskin-Posner, G. Leitus, L. Avram, D. Milstein, Angew. Chem. Int. Ed. 56 (2017) 4229–4233.
[36] U.K. Das, Y. Ben-David, G. Leitus, Y. Diskin-Posner, D. Milstein, ACS Catal. 9 (2019) 479–484.
[37] A.M. Tondreau, J.M. Boncella, Polyhedron 116 (2016) 96–104.
[38] A.V. Polezhaev, C.-H. Chen, Y. Losovyj, K.G. Caulton, Chem. Eur. J. 23 (2017) 8039–8050.
[39] A.V. Polezhaev, C.J. Liss, J. Telser, C.-H. Chen, K.G. Caulton, Chem. Eur. J. 24 (2018) 1330–1341.
[40] A.C. Cabelof, A.M. Erny, V. Carta, M. Pink, K.G. Caulton, Inorg. Chim. Acta 516 (2021) 120118.
[41] M. Mastalir, M. Glatz, N. Gorgas, B. Stöger, E. Pittenauer, G. Allmaier, L.F. Veiros, K. Kirchner, Chem. Eur. J. 22 (2016) 12316–12320.
[42] D. Himmelbauer, B. Stöger, L.F. Veiros, K. Kirchner, Organometallics 37 (2018) 3475–3479.
[43] J. Du Bois, J. Hong, E.M. Carreira, M.W. Day, J. Am. Chem. Soc. 118 (1996) 915–916.
[44] J. Du Bois, C.S. Tomooka, J. Hong, E.M. Carreira, Acc. Chem. Res. 30 (1997) 364–372.
[45] C.L. Hill, F.J. Hollander, J. Am. Chem. Soc. 104 (1982) 7318–7319.
[46] C. Hunt, M. Peterson, C. Anderson, T. Chang, G. Wu, S. Scheiner, G. Ménard, J. Am. Chem. Soc. 141 (2019) 2604–2613.
[47] P. Singh, G. Dutta, I. Goldberg, A. Mahammed, Z. Gross, Inorg. Chem. 52 (2013) 9349–9355.
[48] C. Bolzati, A. Boschi, L. Uccelli, F. Tisato, F. Refosco, A. Cagnolini, A. Duatti, S. Prakash, G. Bandoli, A. Vittadini, J. Am. Chem. Soc. 124 (2002) 11468–11479.
[49] G.P. Connor, B.Q. Mercado, H.M.C. Lant, J.M. Mayer, P.L. Holland, Inorg. Chem. 58 (2019) 10791–10801.
[50] I. Klopsch, M. Finger, C. Würtele, B. Milde, D.B. Werz, S. Schneider, J. Am. Chem. Soc. 136 (2014) 6881–6883.
[51] N.S. Lambic, R.D. Sommer, E.A. Ison, Dalton Trans. 47 (2018) 758–768.
[52] B. Askevold, J.T. Nieto, S. Tussupbayev, M. Diefenbach, E. Herdtweck, M.C. Holthausen, S. Schneider, Nature Chem. 3 (2011) 532–537.
[53] A.F. Cozzolino, J.S. Silvia, N. Lopez, C.C. Cummins, Dalton Trans. 43 (2014) 4639–4652.
[54] C.C. Hojilla Atienza, A.C. Bowman, E. Lobkovsky, P.J. Chirik, J. Am. Chem. Soc. 132 (2010) 16343–16345.
[55] Y. Ishida, H. Kawaguchi, J. Am. Chem. Soc. 136 (2014) 16990–16993.
[56] Z.-J. Lv, J. Wei, W.-X. Zhang, P. Chen, D. Deng, Z.-J. Shi, Z. Xi, Natl. Sci. Rev. 7 (2020) 1564–1583.
[57] J.S. Silvia, C.C. Cummins, J. Am. Chem. Soc. 131 (2009) 446–447.
[58] M. Ding, G.E. Cutsail Iii, D. Aravena, M. Amoza, M. Rouzières, P. Dechambenoit, Y. Losovyj, M. Pink, E. Ruiz, R. Clérac, J.M. Smith, Chem. Sci. 7 (2016) 6132–6140.